ADVANCED FUNCTIONAL MATERIALS
www.afm-journal.de

A Transparent, Smooth, Thermally Robust, Conductive Polyimide for Flexible Electronics

*Joshua A. Spechler, Tae-Wook Koh, Jake T. Herb, Barry P. Rand, and Craig B. Arnold**

In this work, a thermally and mechanically robust, smooth transparent conductor composed of silver nanowires embedded in a colorless polyimide substrate is introduced. The polyimide is exceptionally chemically, mechanically, and thermally stable. While silver nanowire networks tend not to be thermally stable to high temperatures, the addition of a titania coating on the nanowires dramatically increases their thermal stability. This allows for the polyimide to be thermally imidized at 360 °C with the silver nanowires in place, creating a smooth (<1 nm root mean square roughness), conductive surface. These transparent conducting substrate-cum-electrodes exhibit a conductivity ratio figure of merit of 272, significantly outperforming commercially available indium-tin-oxide (ITO)-coated plastics. The conductive polymide is subjected to various mechanical tests and is used as a substrate for a thermally deposited, flexible, organic light-emitting diode, which shows improved device performance compared to a control device made on ITO coated glass.

1. Introduction

Transparent electrodes for flexible electronics pose a unique challenge to the material science community by requiring materials that are concurrently electrically, optically, mechanically, thermally, and chemically stable.[1–3] Typical transparent electrodes used in flat panel displays, organic light-emitting diodes (OLEDs), and solar cells are made from doped metal oxides, especially indium tin oxide (ITO). Layers of ITO are most commonly deposited onto glass substrates, because ITO has excellent adhesion to glass and the high temperatures required to produce highly conductive ITO are not compatible with plastic substrates. Furthermore, ITO is mechanically brittle, making it challenging to incorporate into flexible electronics applications.[4] Thus, transparent substrate-cum-electrodes based on nanocomposites of metals and flexible transparent materials have emerged as a leading candidate to replace ITO.[5–8] Silver nanowire (AgNW) networks, a subclass of these metal nanocomposites, have the added benefits of ease of fabrication from solution, chemical stability both in suspension and in operando, and excellent electrical conduction.[9–12] Additionally, AgNW suspensions in typical organic solvents deposit easily onto a wide range of different transparent substrates, including glass, polyethylenes, and polycarbonates.[13–15] Excellent sheet resistance and transparency can be obtained via the use of high aspect ratio AgNWs, and/or post-processing of the nanowire network to weld the high resistance nanowire–nanowire junctions.[16–19] Networks of AgNWs on both glass and plastic have thus been used at both a research and commercial scale in a variety of applications.

While there are numerous benefits of AgNW networks, there are still limitations. First, the AgNW networks are thermally unstable at temperatures above 250 °C, restricting their use to low temperature applications.[20] Second, the as-deposited AgNW networks typically have very high surface roughness, which limits their use as a bottom electrode upon which subsequent layers are deposited.[21] And finally, AgNW networks exhibit poor adhesion to commonly employed substrates,[22,23] which makes handling and long term use difficult. In this work, we introduce a method to overcome all of the aforementioned limitations with a composite material of AgNWs embedded at the surface of a colorless polyimide substrate that can withstand a thermal imidization at 360 °C. The AgNW network thermal stability is improved via the addition of titania (or TiO_x), from sol–gel. Thermally imidizing the polyimide with the nanowires in place, which is possible with our improved thermal stability of the nanowires, dramatically decreases the surface roughness and allows excellent mechanical properties.

Polyimides are widely used in electronics as mechanically and thermally robust insulators.[24] They are not typically used for transparent substrate materials in light emitting or absorbing devices because the most widely used polyimide, Kapton (DuPont), is strongly absorbing in the shorter visible wavelengths, giving it a characteristic amber hue.[25] Semialicyclic[26] and fluorinated[27] moieties have been suggested to enhance

J. A. Spechler, Prof. C. B. Arnold
Department of Mechanical and Aerospace Engineering
Princeton Institute for the Science and Technology of Materials (PRISM)
Princeton University
Princeton 08544, NJ, USA
E-mail: cbarnold@princeton.edu
Dr. T.-W. Koh, Prof. B. P. Rand
Department of Electrical Engineering
Princeton University
Princeton 08544, NJ, USA
J. T. Herb
Department of Chemistry
Princeton University
Princeton 08544, NJ, USA
Prof. B. P. Rand
Andlinger Center for Energy and the Environment
Princeton University
Princeton 08544, NJ, USA

DOI: 10.1002/adfm.201503342

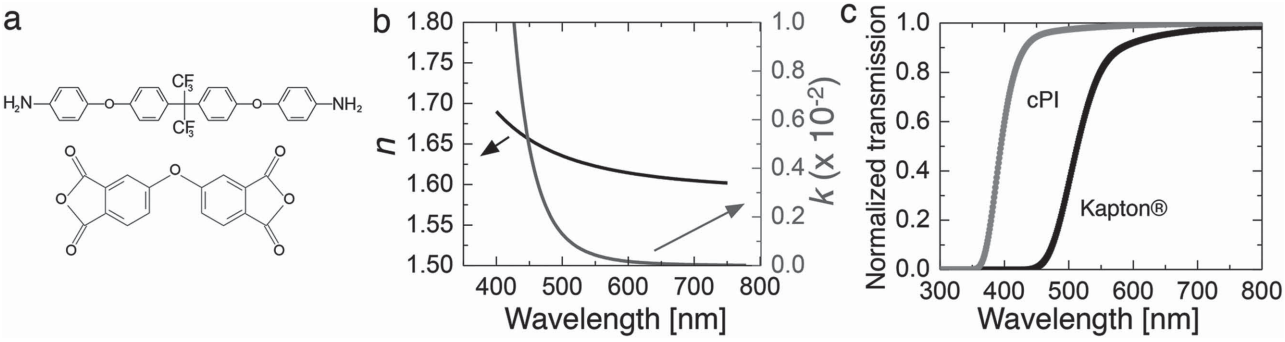

Figure 1. a) The dianiline (upper) and dianhydride (lower) moieties used to create the colorless polyimide (cPI). b) Index of refraction (n) and extinction coefficient (k) for the fully imidized colorless polyimide. c) Transmission spectra normalized to 1 at 800 nm for cPI and Kapton.

visible transmission in polyimides. As such, we synthesize a colorless polyimide from a fluorinated dianiline moiety, and a typical dianhydride moiety. Combining the colorless polyimide with the embedded AgNWs, we create a conductive transparent polyimide suitable as a chemically, thermally, and mechanically robust substrate-cum-electrode.

2. Results and Discussion

2.1. Synthesis and Characterization of the Colorless Polyimide

We synthesize the polyamic acid (polyimide precursor) solution in dimethylacetamide (DMAc) as described in the Experimental Section that, after a curing/imidization step, becomes colorless polyimide (cPI). The specific dianiline and dianhydride moieties used are shown in **Figure 1**a. Figure 1b,c shows the measured optical properties of the cPI: the index of refraction (n), extinction coefficient (k), and transmission spectra. Additionally, in Figure 1c, the transmission is shown for Kapton, which has a measured $n = 1.70$ (at a wavelength of 589 nm)[25] but is simply too absorptive in the blue part of the visible spectrum for use as a transparent substrate. This difference highlights a well-known tradeoff between the index of refraction and absorption of polyimides.[26] While polyimides typically have a very high index of refraction ($n > 1.6$), as the index increases the absorption edge red-shifts, resulting in a more amber-colored polyimide.

The polyimide curing process begins with a prebake step of 20 min at 160 °C to evaporate the DMAc solvent. Then the precursor, a polyamic acid, becomes a polyimide through a condensation reaction (referred to as imidization), which typically takes place at a high temperature. In the case of our colorless formulations, 360 °C for 20 min is suitable to imidize the precursor solution into cPI. This high temperature imidization is a challenge when trying to embed AgNWs within the substrate prior to imidization to ensure a smooth conductor surface. It is well studied that AgNWs break up into nanoparticles through the Rayleigh–Plateau instability at temperatures far below the bulk silver melting point.[20,28,29] In order to prevent the beading up of silver upon imidization, we coat the AgNWs with a thin layer of titania. We deposit the titania from a diluted sol-gel, synthesized in the laboratory atmosphere at room temperature from hydrogen peroxide and titanium (IV) isopropoxide (detailed in the Experimental Section). This method has previously been detailed as an effective way to make ≈2 nm shells of titania around AgNWs without adverse effects to the macroscopic sheet resistance or optical transparency of the resultant electrode.[30] **Figure 2** shows nanowires on glass after thermal cycling at the imidization temperature for cPI (20 min at 160 °C, followed by 20 min at 360 °C) without and

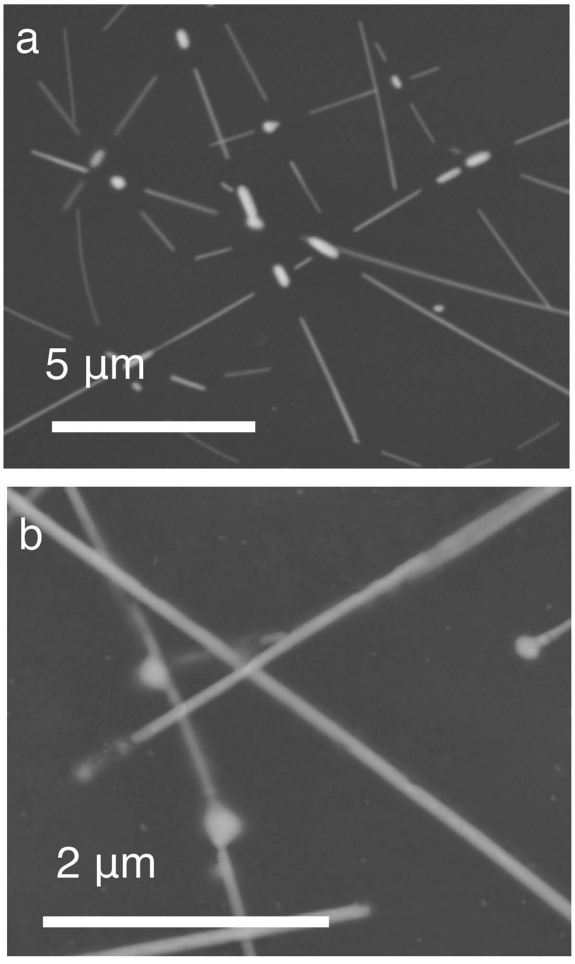

Figure 2. Scanning electron microscope images of AgNWs on glass after thermal cycling of 20 min at 160 °C, followed by 20 min at 360 °C a) without and b) with a titania sol–gel coating. (Note: there is a magnification change between the two images, which serves to show the junctions in (b) remain intact.)

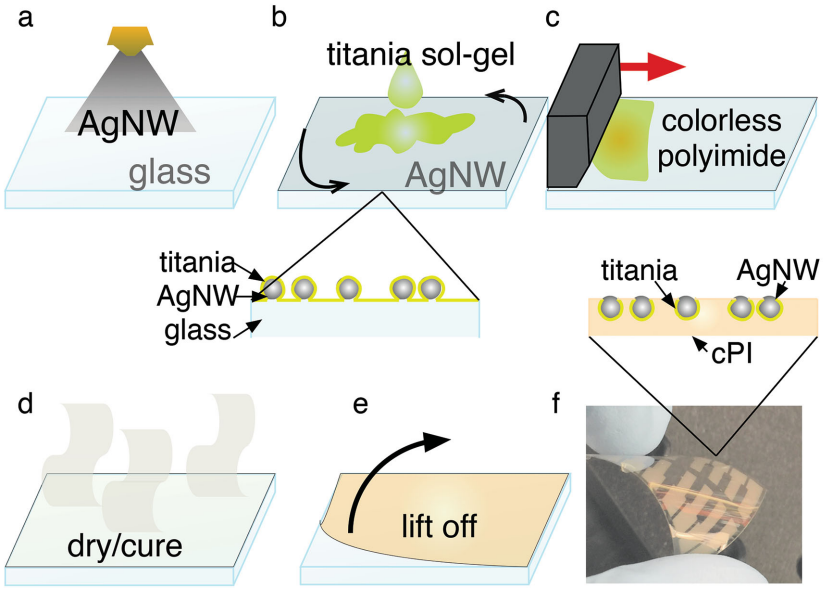

Figure 3. a) Ag NWs are sprayed onto a clean glass slide. b) Titania sol–gel is cast onto the AgNW network. c) A thick viscous layer of colorless polyimide liquid precursor is blade coated onto the glass slide. d) The AgNW/titania/polyimide precursor is cured. e) The polyimide film is lifted from the glass, revealing the buried interface. f) In a photograph the nanowires are visible in a pattern (for device integration) due to their haziness.

with a coating of titania sol-gel. Clearly, the nanowires without the titania have begun to melt and break up into silver droplets destroying the connectivity of the network. Recently, Kim et al. have described a colorless polyimide AgNW composite[31] which can be cured at 200 °C for 1 h, however, the titania sol-gel allows for the use of AgNWs in a wide family of polyimides including Kapton and the cPI used here.

2.2. Fabrication and Characterization of the Conductive Polyimide

With the thermal protection scheme detailed above, we can produce a AgNW, colorless polyimide substrate-cum-electrode fabricated entirely from materials in solution phase. **Figure 3** illustrates the fabrication process; starting with a rigid flat substrate (glass is used here), we deposit AgNWs from suspension via a spray nozzle. After the AgNWs are deposited onto the glass, we post-process the network to increase the conductivity with laser irradiation, described in detail in our previous work.[32,33] The now post-processed nanowire network is spin coated (Figure 3b) with titania sol-gel. After the titania coating, we blade coat (Figure 3c) a viscous layer of colorless polyimide liquid precursor. Typically, the blade is set to about 0.02″ above the substrate, however, the final thickness of the polymer layer is more dependent upon the weight content of the polymer-solids in solution. It is important to note here that no degradation (delamination or otherwise) of the silver nanowire network is observed from either the spin coating or the blade coating procedures. The substrate-cum-electrode stack (glass/AgNW/titania/cPI) is then thermally imidized (Figure 3d) according to the baking method detailed above, after which the substrate can be detached (Figure 3e) at the glass/AgNW interface by soaking in water. The previously buried glass/AgNW interface is highly conductive and smooth. Additionally, shadow masking the glass substrate during the spray coating step is an effective way of patterning the conductive surface of this electrode.[34] Figure 3f shows a final flexible, transparent substrate-cum-electrode which has been patterned for device integration.

We place AgNWs at this buried interface and cure the polyimide on top to mitigate the AgNW roughness and promote better adhesion between the AgNW network and polyimide substrate. Curing the liquid precursor against a rigid flat substrate such as glass provides a very smooth interface. The AgNWs used in this work are on average 90 nm in diameter and 15 µm in length. Thus, when coated on top of a substrate, they exhibit an average root mean square (RMS) surface roughness on the order of 100 nm. **Figure 4**a shows an atomic force microscopy (AFM) image for AgNWs deposited via spray

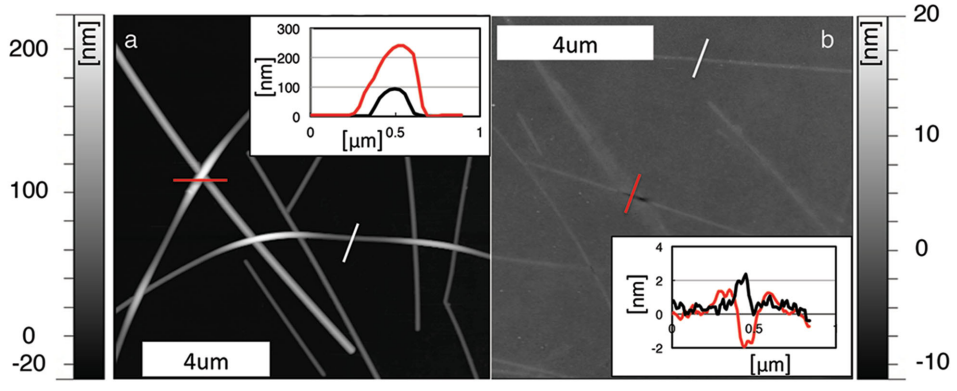

Figure 4. Atomic force microscope images of a) AgNWs spray coated on top of a colorless polyimide substrate. Insets are the profiles marked on the image (the white line in the image corresponds to the black curve in the inset plot). b) AgNWs embedded in colorless polyimide. Insets are the profiles, with background set to 0 nm, marked on the image (white line in the image corresponds to the black curve in the inset plot).

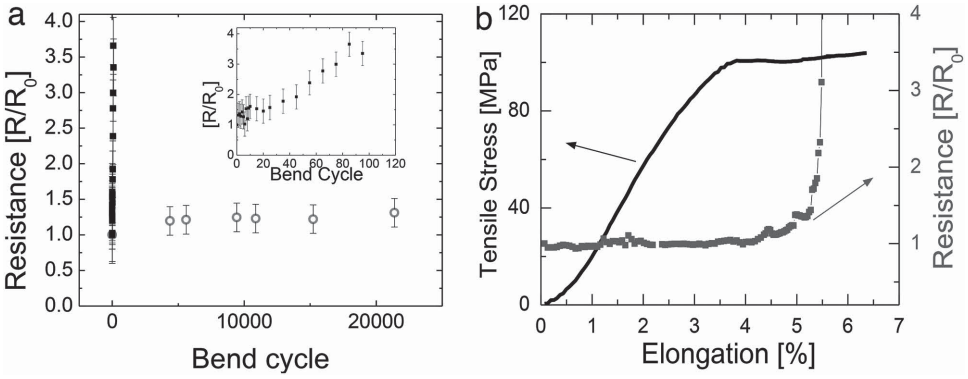

Figure 5. a) Bending fatigue test of colorless polyimide (circles) and AgNWs on top of PET (squares), inset is a zoomed-in view of the AgNWs on PET. b) Tensile test of conductive cPI, the sample is taken to failure with the stress measured (curve) while the resistance is monitored (squares).

coating on top of a cured polyimide substrate. In contrast, Figure 4b shows the once-buried interface between the AgNW network and glass, after the fabrication of a polyimide substrate atop the AgNW network. The surface roughness for the area shown in Figure 4b is <1 nm RMS, and the peak-to-peak height of a AgNW at the polymer surface is only 2 nm (inset profile in Figure 4b). This is lower than AgNWs embedded in other transparent polymer substrates via mechanical pressing which, while smoother than as-deposited AgNWs, typically exhibit a surface roughness on the order of 10 nm RMS.[21,35–37]

The as fabricated substrate-cum-electrode is exceptionally mechanically robust, as demonstrated by a repeated bending test, shown in **Figure 5**a. In the fatigue test, a 1″ × 0.25″ strip of conductive polyimide was bent to ≈1 mm bending radius in an s-shape to both strain the polyimide in tension and compression. This bending was carried out over more than 20 000 cycles over which no loss in conduction was observed via a two-point resistance. This is in contrast to AgNWs spray coated (in same manner as described in the Experimental Section) onto a polyethylene terephthalate (PET) film of 0.01″ thickness. This conductive film was able to bend to the same bending radius, however, after roughly 100 cycles, no conductivity over the film was measured. Upon inspection in a laser scanning confocal microscope it was determined that the conductive PET failed at the contact points to the resistance probe (see Figure S1, Supporting information). The "alligator" style clips slipped and caused the AgNWs to be scratched from the surface. This poor adhesion is a common failure mode for AgNW networks in electronic devices.[17,18] However, the point of contact to our conductive polyimide, upon inspection in the confocal microscope, while indented, shows no delamination of nanowires, suggesting that they are strongly held in the polyimide matrix.

To further test the mechanical properties of our synthesized conductive polyimide, we make a dog-bone shaped sample of conductive cPI, with a cross-sectional area of 1.1 mm^2 and load the sample with 50 MPa of tensile stress (corresponding to an elongation of about 2%), and unload for 100 cycles. After 100 cycles we observe <2% increase in two-point resistance across the dog-bone shaped sample. Finally, we stress the sample in tension to failure, shown in Figure 5b. We observe that the resistance of the sample is unchanged by the elongation until well into the plastic region, wherein after about 5% elongation the sample loses conductivity presumably via breaking of the percolating conduction paths through the silver nanowires at the surface of the polyimide. This sample of polyimide then tears after 6.4% ultimate elongation, the strain rate being 0.033 s^{-1}.

A typical figure of merit for a transparent electrode is the DC/VIS conductivity ratio, first introduced by Grüner and coworkers,[38] which can be calculated from the electrode's optical transparency and the sheet resistance. It is well known that higher areal coverage of nanowires produces a lower sheet resistance, but there will be a transparency trade-off. Further, the use of higher aspect ratio nanowires (particularly nanowires with <60 nm diameter) is best for conductivity at low areal (high transparency) coverage.[19,39] A detailed and thorough assessment of current random nanowire network electrical and optical properties is given by Ye et al.[40] In this work, we have measured conductive polyimide films with sheet resistance as low as 3.4 Ω sq^{-1} (average of 4 locations on a 2.5 cm^2 sample, $\sigma = 0.5$ Ω sq^{-1}) The optical transmission of our conductive polyimide will be predominantly determined by the scattering of the AgNWs. Additionally, the polyimide's high index of refraction will reflect about 6% of normal incidence light (from air) in the visible. The average visible transparency (450–750 nm) for the 3.4 Ω sq^{-1} sample is 69%, (see Figure S2, Supporting Information) giving a DC/VIS conductivity ratio of 272.

2.3. Integration of the Substrate-Cum-Electrode in an OLED Device

The device architecture in **Figure 6**a is that of a green phosphorescent OLED built on top of either a conventional glass substrate with an ITO electrode or a conductive polyimide substrate. The sheet resistance of the conductive polyimide used in this device was measured to be 8 Ω sq^{-1} via a four point probe. On top of the conductive polyimide substrates we spin coat poly(3,4-ethylenedioxythiophene):polystyrene sulfonate (PEDOT:PSS), to ensure even current spreading in the device active area. Additionally, the PEDOT:PSS layer can planarize any pinhole defects or unintended roughness which may have been imprinted from flaws at the sacrificial glass surface. MoO_3 serves as a hole injection layer from both electrodes, and TAPC, TCTA as hole transport layers. The TPBi layer acts as both a host material for the phosphorescent $Ir(ppy)_3$ dopant and as an

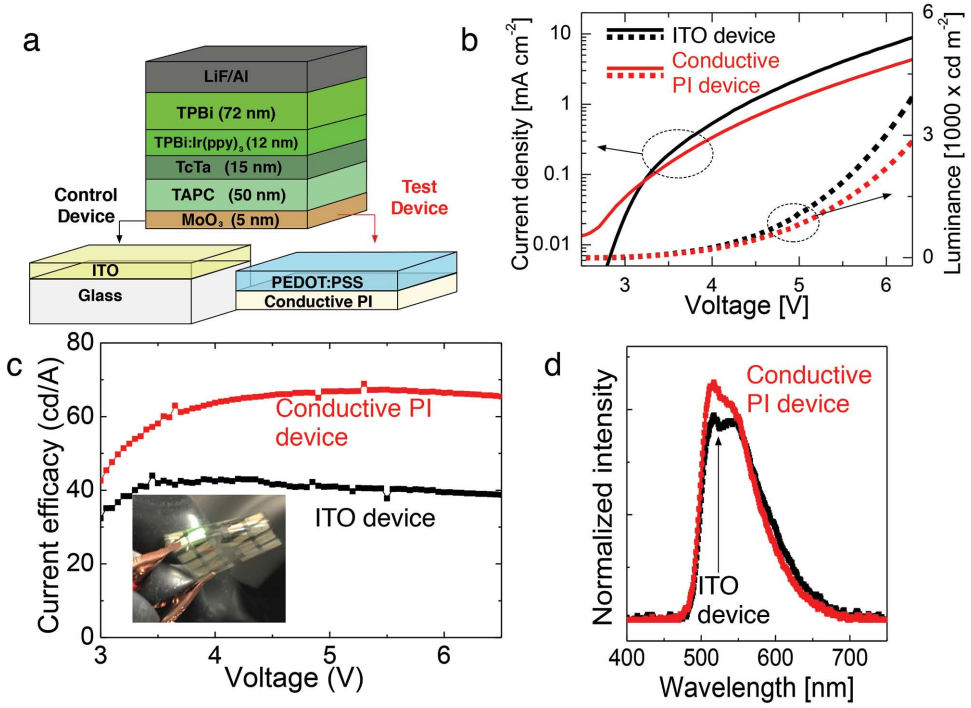

Figure 6. a) Device structure of a green phosphorescent OLED, with control and test transparent conductive electrodes and substrates shown. b) Current density–luminance–voltage behavior of the conductive PI (red curves) and control ITO (black curves) devices. c) Current efficacy of the conductive PI (red) and control ITO (black) devices, inset shows a photograph of the conductive PI device emitting light while being bent. d) Normalized electroluminescence spectra for the conductive PI (red) and control ITO (black) devices.

electron transport layer. A LiF/Al cathode was used for electron injection into the underlying TPBi layer.

The device current density (J)–luminance (L)–voltage (V) characteristics shown in Figure 6b indicate that both the ITO and conductive polyimide samples have the expected diode behavior. However, given that the work function of Ag (≈4.3 eV) is smaller than plasma-treated ITO (≈5.0 eV), together with the additional device series resistance from the PEDOT:PSS, the conductive polyimide device has a lower current density at a given voltage.[16] Despite that the conductive polyimide device is more resistive, the current efficacy, or the forward emission intensity per unit electric current, is about 60% greater than the ITO control at 6 V. This increase in current efficacy of the conductive polyimide device can be attributed to the better charge balance in the device caused by the restrained hole injection from the Ag NW electrode, and also to the haziness of the Ag NW electrode scattering and recovering a certain portion of the waveguided mode in the device. These optical and electrical benefits are unrealizable with unstructured ITO layers, which have the added detriment of being brittle.

3. Conclusion

In conclusion, we have developed a transparent conductive polyimide; transparent due to a fluorinated dianiline moiety, and conductive from embedded silver nanowires. This conductive polyimide layer is mechanically robust, and can be repeatedly bent in tension and compression as well as indented with alligator clips for easy integration with electrical testing equipment. The conductive polyimide is further thermally stable to a temperature of at least 360 °C due to the addition of a sol-gel deposited titania to encase the nanowires. Finally, this conductive polyimide is chemically stable as polyimides are rather chemically inert. The conductive polyimide can be made exceptionally flat with sub-nanometer RMS roughness, making it well suited for use as the bottom layer in a wide variety of devices. In green phosphorescent OLEDs that are vapor deposited on top of the conductive polyimide, we measure a device performance better than control ITO on glass devices. These robust transparent conducting layers are well suited for integration in a range of applications, especially in future flexible optoelectronic devices.

4. Experimental Section

Synthesis of Colorless Polyimide: Polyimides are defined by the polymerization of a dianyhride and dianiline moiety. 98%+ purity [4,4′-oxydiphthalic anhydride] (the dianhydride) and 97%+ purity 2,2-bis[4-(4-aminophenoxy)pheny] hexafluoropropane (the dianiline, all from TCI America) were obtained. Then an equimolar solution of the molecules was prepared in a polar aprotic solvent, anhydrous dimethyl acetamide (DMAc) (Sigma-Aldrich) with approximately 15% by weight solids. The solution was left to stir in the absence of oxygen and water for at least 24 h at room temperature. The result was a viscous liquid polyimide precursor (or polyamic acid) in solution.

Optical Characterization of the Colorless Polyimide: The index of refraction, n, and extinction coefficient, k, were determined on a ≈1 µm thick sample spin cast onto a silicon substrate. The sample was measured in a Woollam M-2000 ellipsometer. The UV–vis absorption

spectra were measured on freestanding samples of the cPI and Kapton, in a Varion Cary 5000 spectrophotometer.

Synthesis of Titania Sol-Gel: 0.5 mL of 30% H_2O_2 (Fisher Scientific) and 9.46 mL of DI water is added to 0.06 mL of titanium tetra-isopropoxide (Sigma-Aldrich). The mixture was left in a sealed vial stirring for at least 48 h at room temperature. The result was a sol-gel, with the consistency of a thick jelly, which easily held small air bubbles when shaken.

Fabrication of the Transparent Conductive Polyimide: Silver nanowires were dispersed in methanol to make an ink with solid weight loading of about 2 mg mL^{-1}. The AgNW ink was then spray coated onto a rigid substrate. The spray nozzle (Badger Air-brush co 350) was fed with nitrogen at 30 psi, and the substrates typically passed under the nozzle about 10 times travelling on a stage at 20 mm s^{-1}. Care was taken to make sure that the nanowire suspension ink was kept agitated for the duration of the spray coating to help prevent agglomeration in the nozzle. The AgNW network was then laser processed to increase the connectivity and thereby conductivity of the network. A 355 nm wavelength laser with 22 ns pulse duration and 100 kHz max rep rate was restored on the AgNW network, where every part of the network was administered with about 100 pulses at 25 mJ cm^{-2} energy fluence. The titania sol-gel was diluted four times by weight with isopropyl alcohol and was then spin cast onto the nanowire network at 2000 rpm for 90 s. After drying, polyamic acid solution was slot dye cast onto the substrate. The whole stack: substrate/Ag NW/titania/polyamic acid was then baked to 360 °C to thermally imidize the polyamic acid. Finally, after baking the conductive polyimide was only weakly bound to the rigid substrate and was removed (occasionally with the aid of soaking in a water bath) leaving a freestanding polyimide substrate electrode. The total thickness of this substrate-cum-electrode depended upon the weight loading of the polyamic acid and the spacing between the slot dye blade and the substrate. Substrates up to 80 μm total thickness were produced.

Mechanical Characterization of the Conductive Polyimide: Repeated bending of a sample of conductive polyimide was carried out on a linear motion stage (LTS-150 ThorLabs), with both mechanical clamps and electrical connections in place during the duration of the testing. The elongation tests were performed in an Instron machine with a 5 kN load cell. The samples for elongation were cut to a dog-bone shape and showed an initial resistance of about 50 Ω. Electrical connections remained in place for the duration of the elongation tests, allowing the resistance to be measured simultaneously with the stress on the polymer sample.

Fabrication of the OLED Device: Prepatterned ITO substrates were cleaned in an ultrasonic bath of soapy water, deionized water, acetone, and isopropanol for 15 min each. Cleaned ITO substrates and the conductive polyimide substrates were treated with oxygen plasma for 5 min to remove organic residues from the surface and to enhance wettability of the aqueous PEDOT:PSS solution. AI4083 PEDOT:PSS (Heraeus) was spin cast onto the conductive polyimide substrates at 2000 rpm for 30 s, and baked at 100 °C for 10 min to remove water. All the substrates were brought into a vacuum thermal evaporation chamber (EvoVac, Angstrom Engineering) for subsequent material deposition of MoO_3 (Alfa Aesar), TAPC (4,4′-cyclohexylidenebis[*N*,*N*-bis(4-methylphenyl)benzenamine], Nichem) TCTA (4,4′,4″-tri(9-carbazoyl)triphenylamine, Nichem), and TPBi (2,2′,2″-(1,3,5-benzinetriyl)-tris(1-phenyl-1-H-benzimidazole), Nichem) doped with $Ir(ppy)_3$ (tris[2-phenylpyridinato-C^2,N]iridium(III), Nichem), TPBi and finally LiF (Sigma-Aldrich)/Al (R. D. Mathis). Base deposition pressure was around 6×10^{-7} Torr. All organic materials were purified before use. Fabricated devices were measured using a Keithley 2400 source-measure unit, a calibrated Si photodiode (FDS-100-CAL, Thorlabs), picoammeter (4140B, Agilent), and a calibrated fiber optic spectrophotometer (UVN-SR, StellarNet Inc.).

Supporting Information

Supporting Information is available from the Wiley Online Library or from the author.

Acknowledgements

The authors acknowledge funding for this work from the DOE EERE SSL program under Award No. #DE-EE0006672. J.A.S. and C.B.A acknowledge support from the Rutgers-Princeton NSF IGERT on Nanotechnology for Clean Energy. Additionally, J.A.S. and C.B.A. acknowledge the support of the National Science Foundation via the MRSEC at Princeton grant DMR-0819860 and the usage of the PRISM Imaging and Analysis Center. B.P.R. acknowledges support from a 3M Nontenured Faculty Award.

Received: August 10, 2015
Revised: September 10, 2015
Published online: November 20, 2015

[1] D. Langley, G. Giusti, C. Mayousse, C. Celle, D. Bellet, J.-P. Simonato, *Nanotechnology* **2013**, *24*, 452001.
[2] K. Ellmer, *Nat. Photonics* **2012**, *6*, 809.
[3] D. S. Hecht, L. Hu, G. Irvin, *Adv. Mater.* **2011**, *23*, 1482.
[4] D. S. Ginley, J. D. Perkins, in *Handbook of Transparent Conductors* (Eds: D. S. Ginley, H. Hosono, D. C. Paine), Springer, New York, NY, USA **2011**, p. 1.
[5] P. Lee, J. Ham, J. Lee, S. Hong, S. Han, Y. D. Suh, S. E. Lee, J. Yeo, S. S. Lee, D. Lee, S. H. Ko, *Adv. Funct. Mater.* **2014**, *24*, 5671.
[6] S. Hong, H. Lee, J. Lee, J. Kwon, S. Han, Y. D. Suh, H. Cho, J. Shin, J. Yeo, S. H. Ko, *Adv. Mater.* **2015**, *27*, 4744.
[7] C. K. Jeong, J. Lee, S. Han, J. Ryu, G.-T. Hwang, D. Y. Park, J. H. Park, S. S. Lee, M. Byun, S. H. Ko, K. J. Lee, *Adv. Mater.* **2015**, *27*, 2866.
[8] K. K. Kim, S. Hong, H. M. Cho, J. Lee, Y. D. Suh, J. Ham, S. H. Ko, *Nano Lett.* **2015**, *15*, 5240.
[9] S. De, T. M. Higgins, P. E. Lyons, E. M. Doherty, P. N. Nirmalraj, W. J. Blau, J. J. Boland, J. N. Coleman, *ACS Nano* **2009**, *3*, 1767.
[10] L. Hu, H. S. Kim, J. Lee, P. Peumans, Y. Cui, *ACS Nano* **2010**, *4*, 2955.
[11] S. M. Bergin, Y.-H. Chen, A. R. Rathmell, P. Charbonneau, Z.-Y. Li, B. J. Wiley, *Nanoscale* **2012**, *4*, 1996.
[12] R. M. Mutiso, K. I. Winey, *Phys. Rev. E* **2013**, *88*, 032134.
[13] J. Jiu, T. Sugahara, M. Nogi, T. Araki, K. Suganuma, H. Uchida, K. Shinozaki, *Nanoscale* **2013**, *5*, 11820.
[14] J. Jiu, M. Nogi, T. Sugahara, T. Tokuno, T. Araki, N. Komoda, K. Suganuma, H. Uchida, K. Shinozaki, *J. Mater. Chem.* **2012**, *22*, 23561.
[15] T. Tokuno, M. Nogi, M. Karakawa, J. Jiu, T. T. Nge, Y. Aso, K. Suganuma, *Nano Res.* **2011**, *4*, 1215.
[16] R. M. Mutiso, M. C. Sherrott, A. R. Rathmell, B. J. Wiley, K. I. Winey, *ACS Nano* **2013**, *7*, 7654.
[17] J. Jiu, T. Araki, J. Wang, M. Nogi, T. Sugahara, S. Nagao, H. Koga, K. Suganuma, E. Nakazawa, M. Hara, H. Uchida, K. Shinozaki, *J. Mater. Chem. A* **2014**, *2*, 6326.
[18] J. Lee, P. Lee, H. Lee, D. Lee, S. S. Lee, S. H. Ko, *Nanoscale* **2012**, *4*, 6408.
[19] J. Lee, P. Lee, H. B. Lee, S. Hong, I. Lee, J. Yeo, S. S. Lee, T.-S. Kim, D. Lee, S. H. Ko, *Adv. Funct. Mater.* **2013**, *23*, 4171.
[20] D. P. Langley, M. Lagrange, G. Giusti, C. Jiménez, Y. Bréchet, N. D. Nguyen, D. Bellet, *Nanoscale* **2014**, *6*, 13535.
[21] W. Gaynor, S. Hofmann, M. G. Christoforo, C. Sachse, S. Mehra, A. Salleo, M. D. McGehee, M. C. Gather, B. Lüssem, L. Müller-Meskamp, P. Peumans, K. Leo, *Adv. Mater.* **2013**, *25*, 4006.
[22] K. Zilberberg, F. Gasse, R. Pagui, A. Polywka, A. Behrendt, S. Trost, R. Heiderhoff, P. Görrn, T. Riedl, *Adv. Funct. Mater.* **2014**, *24*, 1671.
[23] Y. Jin, L. Li, Y. Cheng, L. Kong, Q. Pei, F. Xiao, *Adv. Funct. Mater.* **2015**, *25*, 1581.
[24] *Polyimides: Fundamentals and Applications* (Eds: M. K. Ghosh, K. L. Mittal), Marcel Dekker Inc, New York, NY, USA **1996**.

[25] DuPont, "Kapton properties spec sheet", http://www.dupont.com/content/dam/assets/products-and-services/membranes-films/assets/DEC-Kapton-general-specs.pdf (accessed: July 2015).
[26] T. Higashihara, M. Ueda, *Macromolecules* **2015**, *48*, 1915.
[27] C. Yang, R. Chen, K. Hung, *Polymer* **2001**, *42*, 4569.
[28] E. C. Garnett, W. Cai, J. J. Cha, F. Mahmood, S. T. Connor, M. Greyson Christoforo, Y. Cui, M. D. McGehee, M. L. Brongersma, *Nat. Mater.* **2012**, *11*, 241.
[29] T.-B. Song, N. Li, *Electronics* **2014**, *3*, 190.
[30] W.-F. Xu, M.-C. Tsai, P.-H. Fu, T.-Y. Huang, S.-J. Yang, W.-C. Tian, C.-W. Chu, D.-W. Huang, P.-K. Wei, *RSC Adv.* **2015**, *5*, 18990.
[31] Y. Kim, T. I. Ryu, K.-H. Ok, M.-G. Kwak, S. Park, N.-G. Park, C. J. Han, B. S. Kim, M. J. Ko, H. J. Son, J.-W. Kim, *Adv. Funct. Mater.* **2015**, *25*, 4580.
[32] J. A. Spechler, C. B. Arnold, *Appl. Phys. A* **2012**, *108*, 25.
[33] J. A. Spechler, K. A. Nagamatsu, J. C. Sturm, C. B. Arnold, *ACS Appl. Mater. Interfaces* **2015**, *7*, 1556.
[34] C. Girotto, B. P. Rand, S. Steudel, J. Genoe, P. Heremans, *Org. Electron.* **2009**, *10*, 735.
[35] Q. Zhang, Y. Di, C. M. Huard, L. J. Guo, J. Wei, J. Guo, *J. Mater. Chem. C* **2015**, *3*, 1528.
[36] B.-Y. Wang, T.-H. Yoo, J. W. Lim, B.-I. Sang, D.-S. Lim, W. K. Choi, D. K. Hwang, Y.-J. Oh, *Small* **2015**, *11*, 1905.
[37] C.-H. Song, K.-H. Ok, C.-J. Lee, Y. Kim, M.-G. Kwak, C. J. Han, N. Kim, B.-K. Ju, J.-W. Kim, *Org. Electron.* **2015**, *17*, 208.
[38] L. Hu, D. Hecht, G. Grüner, *Nano Lett.* **2004**, *4*, 2513.
[39] J. H. Lee, P. Lee, D. Lee, S. S. Lee, S. H. Ko, *Cryst. Growth Des.* **2012**, *12*, 5598.
[40] S. Ye, A. R. Rathmell, Z. Chen, I. E. Stewart, B. J. Wiley, *Adv. Mater.* **2014**, *26*, 6670.